Mapping of Explicit Atom onto United Atom Potentials

John D. McCoy*

Department of Materials and Metallurgical Engineering, New Mexico Institute of Mining and Technology, Socorro, New Mexico 87801

John G. Curro

Sandia National Laboratories, Albuquerque, New Mexico 87185

Received July 7, 1998; Revised Manuscript Received October 23, 1998

ABSTRACT: Reversible work, also known as the potential of mean force, is used to map explicit atom (EA) onto united atom (UA) potentials for CH, CH_2, CH_3, and CH_4 sites. These UA potentials are found to be temperature dependent and to be described by stretched exponential-6 functions. Although this is fairly dissimilar to the Lennard-Jones 6−12 potential, the one may be mapped onto the other by requiring that the second virial coefficients and locations of the potential minimum be equal for the two forms. When this is done, good agreement with standard UA potentials is found.

1. Introduction

In recent years there have been significant advances made in the techniques used to perform statistical mechanical computations on realistic molecular models of polymer systems. These methods include Monte Carlo (MC) and molecular dynamics (MD) simulations of multiple chain systems,[1] as well as the application of integral equation methods to polymers in the condensed phase.[2] The limiting factor in the ability of these simulations or computations to model real systems is not so much the statistical mechanical aspect of the problem, but a limited knowledge of the interatomic potentials.

An atomistic level model of a polymer chain would be expected to include *explicit atom* pair interactions (EA) between atoms on the same chain, as well as between atoms on different macromolecules. Such EA interaction potential functions are assumed to be known from ab initio calculations or are obtained from experimental data. In practice, they are finely tuned to capture crystalline properties.

From a computational standpoint, however, it is much more efficient to employ *united atom* interactions (UA) in which, for example, the hydrogen and carbon atoms are combined into a single united atom site. A significant problem with the UA approach is that, at least in principle, the UA potentials no longer have the universality of EA potentials in that they are not always transferable from one polymer to another. One facet of this is that UA potentials would be expected to show a dependence on temperature and, consequently, have only a limited thermal transferability. The limitations of UA models are well-known and have been emphasized recently by Boyd and co-workers.[3] On the other hand and in apparent contradiction, UA potentials have been more successful than EA potentials at describing the liquid−vapor equilibrium of normal alkanes.[4,5] This implies (1) that the temperature variations in UA potentials saturate at high temperature and (2) that the additional number of parameters in EA potentials makes fitting to liquid−vapor data tedious.

The purpose of the present investigation is to show that it is possible to perform an approximate mapping from explicit atom potentials to a united atom potential for sites characteristic of polyolefin molecules in a manner that accounts for the local chain structure as well as for temperature effects. This mapping involves a simple Monte Carlo simulation of a pair of molecules composed of the sites of interest and described by an EA force field. Although pair correlation functions, $g(r)$, are equated in the mapping process (the UA $g(r)$ equals the EA carbon−carbon $g(r)$), not all properties are as carefully conserved. A great deal of work will be necessary in order to quantify this procedure's implications to, for instance, the density and chain length dependencies of the resulting UA potentials. Here we have focused on the UA functional form and its temperature dependence.

In particular, we have demonstrated this procedure for CH_4, CH_3, CH_2, and CH moieties in which the hydrogens are absorbed into united atom sites. For purposes of demonstration, we performed our mapping calculations for three different sets of semiempirical explicit atom potentials between CC, HH, and CH atom pairs: (1) the exp-6 Dreiding force field of Mayo, Olafson, and Goddard [6] (MOG), (2) the Lennard-Jones approximation to this Dreiding force field [6] (LJ-MOG), and (3) the exp-6 force field of Sorensen, Liau, Kesner, and Boyd[7] (SLKB).

Our motivation for investigating possible mappings between explicit atom and united atom potentials is to enable the development of compatible EA and UA potential sets. To investigate the feasibility of such an approach, we perform the EA/UA mapping on selected explicit atom force fields. We then compare with some of the recent united atom potentials developed from various comparisons with experimental data. There are a wide range of such UA potentials available; however, the potentials from the recent work of Siepmann et al.[4] and of Nath et al.[5] obtained from phase diagrams of alkanes probably provide the most realistic UA potentials.

The proposed EA/UA mapping formalism is based on our previously developed[8] reversible work (or potential

* To whom mail should be addressed.

10.1021/ma981060g CCC: $15.00
Published on Web 12/09/1998

of mean force) technique in which averages are taken over angular orientations. In this manner an entropic repulsion involving the "meshing" of the hydrogen atoms is built into the resulting UA potential. Specifically, as we showed previously,[8] the explicit atom interactions between pairs of atoms in two hard-site "methane" molecules translate into a UA potential containing a soft repulsion superimposed on a hard core.

For a fully interacting system with both attractions and repulsions, temperature effects would be more pronounced. One would expect that, at low temperature, the packing would minimize the energy, resulting in a highly meshed structure with a large well depth. On the other hand, at high temperature, entropy plays a more dominant role, and the low-energy, low-entropy structures which are of importance at low temperature are no longer preferentially populated. This would lead to an increase in well location and a decrease in the energetic contribution to the site−site interaction. In practice, as the temperature is increased, we find that while the well location does tend to increase, the entropic contribution to the site−site free energy causes a modest increase in the net depth of the well. Consequently, UA simulations can be envisioned that correctly account for variations in both temperature and chain structure: this, again, is the eventual goal of the current study.

In this paper we begin by describing the reversible work method of mapping. We then show the EA/UA mapping results for the various polyolefin sites obtained from the three explicit atom potentials. These results will then be discussed in terms of well-known united atom potentials.

2. Explicit Atom to United Atom Mapping

The concept of reversible work is well-known and is described in standard liquid-state texts.[9] In a typical application, the distance between two tagged interaction sites is held fixed while other degrees of freedom in the system (typically, the location of other particles) are allowed to vary. The constrained partition function is then calculated and associated with the reversible work $w(r)$ by the relation

$$e^{-\beta w(r)} = \frac{\sum_i e^{-\beta U_i(r)}}{\sum_i e^{-\beta U_i(\infty)}} \tag{2.1}$$

where β is $1/kT$ and $U(r)$ is the total potential energy of the system with the two sites fixed at a distance r apart. The summations are over all states i in keeping with the constraint on the tagged sites. This ensures, by construction, that a dilute gas of particles interacting with a potential $w(r)$ will have the same pair correlation function as the system of high-density considered in eq 2.1.

This methodology of embodying many body effects in an effective potential, the reversible work, can be extended to the problem at hand in a relatively straightforward manner. Consider two methane molecules interacting with EA pair potentials with the carbon atoms separated by a distance r. Since the system consists of only these two molecules, and since the potential energy approaches zero as r becomes large, eq 2.1 reduces to the angle average of the Boltzmann factor according to

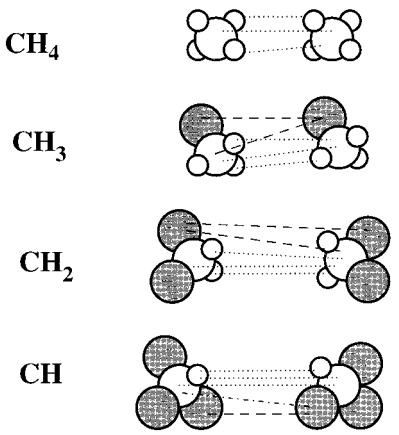

Figure 1. Details of interactions used in calculations. The dashed lines represent EA interactions, the dotted, UA interactions; and the dot−dashed, the geometric mean of two UA potentials. The shaded spheres are CH_3 UA's except for the CH_2 case where they are CH_2 UA's.

$$e^{-\beta w(r)} = \langle e^{-\beta U(r)} \rangle \tag{2.2}$$

where $\langle ... \rangle$ denotes an average over all angular orientations of both molecules subject to the constraint that the carbon atoms are separated by r. Although the above result is appropriate to the gas phase, the EA potentials should be, to a good approximation, independent of density, resulting in a density-independent UA potential $w(r)$. On the other hand, the united atom potential or reversible work, $w(r)$, defined by eq 2.2, is inherently temperature dependent. In the evaluation of eq 2.2 the explicit atom potentials are used in the computation of $U(r)$. A pictorial description of the methane EA/UA mapping calculation is illustrated in Figure 1 where the dotted lines indicate the various explicit atom pair potentials.

In the case of methane, the mapping is well-defined by eq 2.2; however, in the case of united atom sites used to construct a larger molecule, the immediate environment of the site in question needs to be taken into account. To compute the united atom potential of a CH_3 united atom site, we consider a pair of ethane molecules as illustrated in Figure 1. While the reversible work formalism does not exclude a mapping from a full EA description, we, for expedience, have considered a mapping from the following hybrid EA-UA structure. Each ethane molecule is composed of an explicit atom CH_3 bonded to a united atom CH_3 site, shown as shaded in the figure. The total potential energy of the pair of molecules is given by the sum of (1) explicit atom interactions between all C and H pairs illustrated by the dotted lines, (2) united atom potentials $w(r)$ between shaded sites indicated by dashed lines, and (3) cross interactions between the explicit atom CH_3 on one molecule with the united atom CH_3 on the other which we also approximate by a united atom potential $w(r)$. The reversible work $w(r)$ for this system is found from the ratio of two angular averages,

$$e^{-\beta w(r)} = \frac{\langle e^{-\beta U(r)} \rangle}{\langle e^{-\beta U(r)} \rangle_0} \tag{2.3}$$

where the subscript zero refers to the angular average with the explicit atom interactions (corresponding to the "direct" interactions) turned off. Since the united atom potential $w(r)$ appears on both sides of eq 2.3, the calculation must be done in a self-consistent manner. This is accomplished by assuming an initial form for $w(r)$ for the purpose of computing $U(r)$, followed by computation of a new $w(r)$ from eq 2.3. The procedure is iterated until a self-consistent $w(r)$ is found. In practice, convergence of the reversible work is achieved after a few iterations, although it is necessary to use a fine spacing of points ($\sim$0.01 Å) in $w(r)$.

The CH_2 and CH sites are treated in a similar manner as indicated in Figure 1. The shaded sites are treated as sites interacting with united atom potentials $w(r)$ that are determined self-consistently through eq 2.3. For the CH case the CH_3 UA potentials[10] are of the Lennard-Jones form with well depth of 80.51 K and minimum location of 4.39 Å. In all cases, the denominator in eq 2.3 serves the purpose of "zeroing-out" the indirect interactions and is related to the cavity distribution function employed in liquid-state theory.[9]

In general, eq 2.3 will result in a $w(r)$ dependent upon the auxiliary sites. For instance, as is usually, although not always, found in the UA modeling of polyolefins,[4,5,10] the potential of the CH_3 site varies from ethane to *n*-butane. While we have varied the description of the auxiliary sites and find that it does have an effect on the calculated UA potential, it was felt that a detailed study of this subtle effect should be conducted at a latter point with a mapping from a full EA description of the molecules.

Although we have made a number of expedient approximations, they are, in principle, not necessary. In particular, the reversible work formalism discussed above can be implemented with the full EA description of the molecules and in a melt environment. Although we do not believe that such refinements would substantially change the resulting UA potentials in most cases, it is important that the reader realize that the underlying formalism is capable of accurately describing a high level of system specific detail. An instance where such detail would be imperative is the application of our formalism to explicit atom potentials that use partial charges since this would necessitate a liquid environment in order to provide the correct dielectric screening of the charges.

3. Results

In this paper we present results for the united atom potentials for CH_4, CH_3, CH_2, and CH sites. These UA potentials could, in principle, be employed in simulations of polyolefin melts and blends. The angular averages in eq 2.2 or 2.3 were carried out as a function of carbon−carbon separation r in a self-consistent manner to map out the various united atom potentials. Here we present results obtained by using the three explicit atom potentials mentioned in the Introduction: MOG, LJ-MOG, and SLKB. In all cases, the bond lengths and bond angles were rigid with a carbon−carbon bond length of 1.53 Å and a hydrogen−carbon bond length of 1.09 Å. All bond angles were strictly tetrahedral.

The MOG and SLKB potentials are of the exp-6 form given by

$$u(r) = \epsilon\left[\left(\frac{6}{\zeta - 6}\right)\exp\left[\zeta(1 - (r/R_0)) - \left(\frac{\zeta}{\zeta - 6}\right)(r/R_0)^{-6}\right]\right] = A\exp(-Cr) - Br^{-6} \quad (3.1)$$

where ϵ is the well depth, R_0 is the location of the minimum, and ζ is a scaling parameter. The parameters A, B, and C can be expressed in terms of ϵ, R_0, and ζ. The various parameters in the MOG and SLKB potentials are given in Table 1. Following standard practice, the cross interactions are taken to be

$$A_{ij} = [A_{ii}A_{jj}]^{1/2}$$
$$B_{ij} = [B_{ii}B_{jj}]^{1/2}$$
$$C_{ij} = {}^1/_2[C_{ii}C_{jj}] \quad (3.2)$$

The LJ-MOG and the various united atom potentials are of the Lennard-Jones form written as

$$u(r) = \epsilon\left[\left(\frac{r}{R_0}\right)^{-12} - 2\left(\frac{r}{R_0}\right)^{-6}\right] \quad (3.3)$$

The common united atom Lennard-Jones parameters are summarized in Tables 2−5 for the sites of interest. The parameters ϵ and R_0 for the LJ-MOG potentials are taken to be the same as those of the MOG potentials.

In Figure 2, we present the united atom potentials calculated by the reversible work procedure for each of the four united atom sites at $T = 300$ K. The MOG explicit atom potential was employed in the calculation. It is particularly interesting that the form of the resulting UA potentials is neither of the Lennard-Jones nor of the usual exp-6 form, although an exp-6 with a large ζ provides a reasonable description for high temperatures ($T > 200$ K). The variation with temperature for the CH_2 case is shown in the insert. The form of the CH potential is particularly complex and is only crudely fit by any of the functions.

The location of the minimum, R_0, at 300 K is plotted in Figure 3 as a function of N, the number of hydrogens absorbed in the united atom sites. Results are shown for all three explicit atom potentials. Also plotted in this figure are the R_0 values found from several united atom potentials. It can be seen that both the MOG and LJ-MOG are in remarkable agreement with the united atom potentials. Note that the SLKB explicit atom potential leads to UA R_0 values that are consistently low in comparison. This appears to arise from the strong C/H cross term in the SLKB force field. It is also interesting to note that the position of the minimum is slightly larger for the CH_2 sites than for the other united atom groups.

Figure 4 shows our results for the well depth ϵ as a function of the number of hydrogens. All three of the explicit atom potentials appear to give well depths considerably larger than would be expected on the basis of the united atom potentials. Indeed, they appear to simply interpolate between the well depths of the methane and the bare carbon interactions.

4. Discussion

The apparent largeness of the well depths predicted from our mapping is, at least in part, a consequence of the *assumed* Lennard-Jones form of the united atom

Table 1. Explicit Atom Potentials

interaction pair	R_0 (Å)	ϵ (K)	ζ	ref
Mayo, Olafson, and Goddard				
CC	3.8983	47.86	14.034	6
CH	3.539	18.93	13.228	6
HH	3.195	7.65	12.382	6
Sorensen, Liau, Kesner, and Boyd				
CC	3.872	47.58	11.97	7
CH	3.370	25.66	12.60	7
HH	3.253	4.93	11.11	7

Table 2. United Atom Potentials for CH_4

first author	R_0 (Å)	ϵ (K)	B(300 K) (cm^3/mol)	d_{WCA} (300 K) (Å)	ref (year)
Hirshfelder	4.28	148.0	−41.5	3.79	14 (1954)
Jorgensen	4.187	147.90	−38.8	3.71	10 (1984)
Ben-Amotz	4.187	142.0	−34.6	3.70	15 (1990)
Mayo	4.2370	151.8	−43.0	3.76	6 (1990)
van der Vegt	4.187	150.0	−40.9	3.71	16 (1993)
Matyushov	4.22	170.0	−55.9	3.76	17 (1996)
Daura	4.16	152.0	−40.9	3.69	23 (1998)
MOG	4.290	142.3 (127.9)	−26.9	3.75	this work
LJ-MOG	4.385	135.3 (115.2)	−19.0	3.85	this work
SLKB	4.153	159.7 (153.4)	−41.6	3.61	this work

Table 3. United Atom Potentials for CH_3

first author	R_0 (Å)	ϵ (K)	B(300K) (cm^3/mol)	d_{WCA} (300K) (Å)	ref (year)
Dunfield	4.254	90.60	−1.2	3.68	18 (1978)
Jorgensen	4.333	90.6	−1.3	3.74	19 (1981)
Jorgensen (ethane)	4.237	104.2	−9.9	3.69	10 (1984)
Jorgensen (*n*-butane)	4.383	88.1	0.5	3.78	10 (1984)
Jorgensen (isobutane)	4.445	73.0	11.0	3.80	10 (1984)
Jorgensen (neopentane)	4.389	80.5	5.6	3.77	10 (1984)
Mayo	4.153	125.8	−23.1	3.65	6 (1990)
Lopez-Rodriguez	4.153	116.0	−16.8	3.63	20 (1993)
Lopez-Rodriguez	4.403	104.0	−10.9	3.83	20 (1993)
Siepmann	4.411	114.0	−18.4	3.86	4 (1993)
Siepmann	4.232	98.1	−6.0	3.67	4 (1997)
Siepmann	4.209	98.0	−5.8	3.65	4 (1998)
Nath (ethane)	4.293	100.6	−7.9	3.73	5 (1998)
Nath (propane)	4.329	102.6	−9.4	3.76	5 (1998)
Nath (*n*-butane and up)	4.389	104.0	−10.82	3.82	5 (1998)
Daura	4.350	88.1	0.4	3.75	23 (1998)
MOG	4.325	114.5 (94.1)	−3.6	3.77	this work
LJ-MOG	4.415	109.3 (85.3)	2.4	3.86	this work
SLKB	4.189	130.3 (114.8)	−16.4	3.64	this work

potentials developed in the literature. This is clearly a problem since the united atom potentials arising from our mapping, particularly their repulsive branches, are not describable with the Lennard-Jones form. Indeed, for the UA potentials to be of a Lennard-Jones 6−12 form, the corresponding EA force field would need to be of an extremely unusual type.

To make a sensible comparison with the known Lennard-Jones UA potentials, we chose a Lennard-Jones equivalent well depth, ϵ_{LJ}, which forces agreement between a Lennard-Jones potential and the actual united atom potentials resulting from our EA/UA mapping. This was done on a thermodynamic basis through the second virial coefficient, $B(T)$. This quantity is

Table 4. United Atom Potentials for CH_2

first author	R_0 (Å)	ϵ (K)	B(300K) (cm^3/mol)	d_{WCA}(300K) (Å)	ref (year)
Ryckaert	4.403	72.0	11.3	3.76	21 (1978)
Dunfield	4.445	70.4	12.7	3.79	18 (1978)
Weber	4.501	59.4	20.7	3.80	22 (1979)
Jorgensen	4.467	55.4	22.8	3.76	19 (1981)
Jorgensen	4.383	59.4	19.1	3.70	10 (1984)
Mayo	4.068	99.8	−6.3	3.53	6 (1990)
Lopez-Rodriguez	4.153	56.8	17.5	3.50	20 (1993)
Lopez-Rodriguez	4.403	49.7	25.1	3.69	20 (1993)
Siepmann	4.411	47.0	26.8	3.68	4 (1993)
Siepmann	4.434	46.0	27.8	3.70	4 (1997)
Nath	4.411	45.8	27.5	3.68	5 (1998)
Daura	4.400	58.9	19.6	3.72	23 (1998)
MOG	4.366	89.9 (63.3)	16.5	3.82	this work
LJ-MOG	4.445	86.8 (55.4)	22.4	3.92	this work
SLKB	4.226	104.4 (82.4)	3.8	3.69	this work

Table 5. United Atom Potentials for CH

first author	R_0 (Å)	ϵ (K)	B(300K) (cm^3/mol)	d_{WCA}(300K) (Å)	ref (year)
Dunfield	4.748	65.4	19.7	4.03	18 (1978)
Jorgensen	4.770	25.2	47.5	3.84	19 (1981)
Jorgensen	4.321	40.2	28.7	3.58	10 (1984)
Mayo	4.983	73.8	7.4	3.41	6 (1990)
Daura	4.265	37.7	28.8	3.52	23 (1998)
MOG	4.330	67.8 (36.2)	30.8	3.77	this work
LJ-MOG	4.400	65.3 (30.9)	34.8	3.89	this work
SLKB	4.200	79.1 (49.4)	21.9	3.67	this work

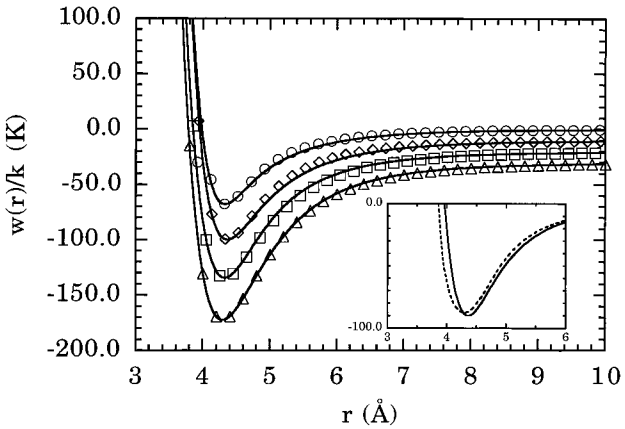

Figure 2. Calculated UA potentials for the MOG EA force field. The primary figure shows the results at 300 K: the circles are for CH, the diamonds for CH_2, the squares for CH_3, and the triangles for CH_4. The curves are displaced in increments of 10 K for ease of viewing. The insert shows the change with temperature for CH_2: the solid line is at 300 K and the dashed line at 50 K.

conveniently computed from

$$B(T) = 2\pi N_A \int_0^\infty [1 - e^{-\beta w(r)}] r^2 \, dr \qquad (4.1)$$

where N_A is Avogadro's number. First, $B(T)$ was found numerically using the united atom potentials for the various sites obtained from the mapping. The position R_0 of the minimum in $w(r)$ was taken from the mapping procedure as a function of temperature. The well depth ϵ was then adjusted in the Lennard-Jones potential for $w(r)$ in eq 4.1 until the same second virial coefficient was obtained. The resulting LJ−UA potential for an

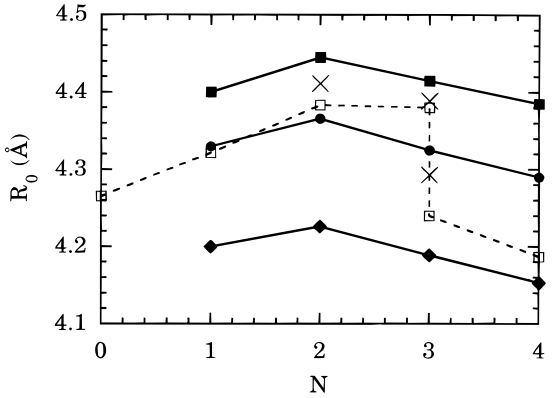

Figure 3. Well location at 300 K vs number of hydrogens in the UA site. The open squares are from Jorgensen et al.[10] The X's are from Nath et al.[5] The filled squares are the LJ-MOG averages. The filled circles are the MOG averages. The filled diamonds are the SLKB averages. Where available, CH_2 results for both ethane and *n*-butane are reported.

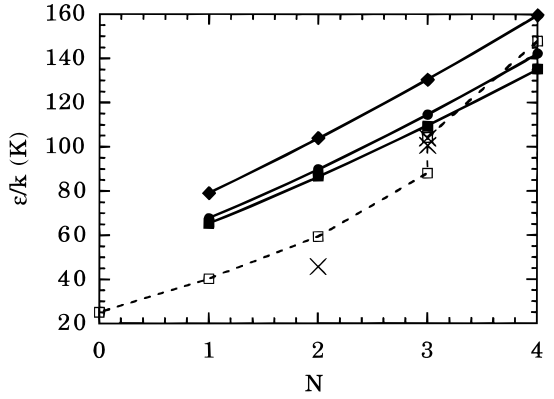

Figure 4. Well depth at 300 K vs number of hydrogens in the UA site. The open squares are from Jorgensen et al.[10] The X's are from Nath et al.[5] The filled squares are the LJ-MOG averages. The filled circles are the MOG averages. The filled diamonds are the SLKB averages. Where available, CH_2 results for both ethane and *n*-butane are reported.

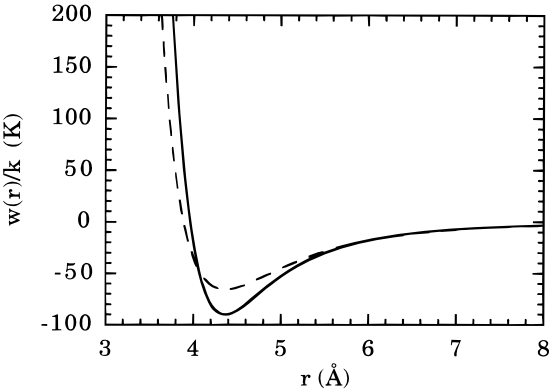

Figure 5. Comparison of full (solid line) and Lennard-Jones fitted (dashed line) average potentials for the MOG CH_2 force field at 300 K.

example case is shown in comparison with the full UA potential in Figure 5. The results of the mapping procedure at 300 K are listed in Tables 2−5 with the Lennard-Jones well depth in parentheses.

The Lennard-Jones well depths are depicted in Figures 6 and 7 at $T = 300$ and 450 K, respectively, as a function of the number of hydrogens in each site. In Figure 6 we observe that excellent agreement is found between the standard united atom potentials[10] and the

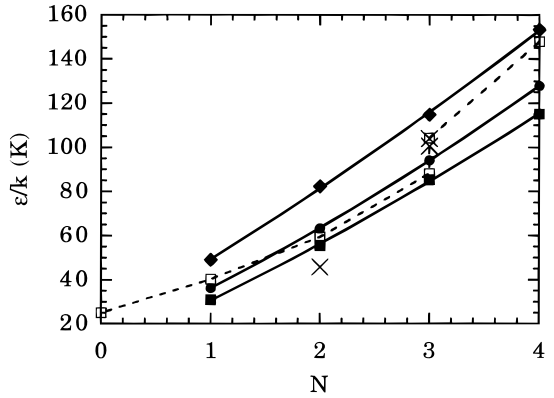

Figure 6. Well depth at 300 K vs number of hydrogen in UA site. The open squares are from Jorgensen et al.[10] The X's are from Nath et al.[5] The filled squares are the LJ fits of the LJ-MOG averages. The filled circles are the LJ fits of the MOG averages. The filled diamonds are the LJ fits of the SLKB averages. Where available, CH_2 results for both ethane and *n*-butane are reported.

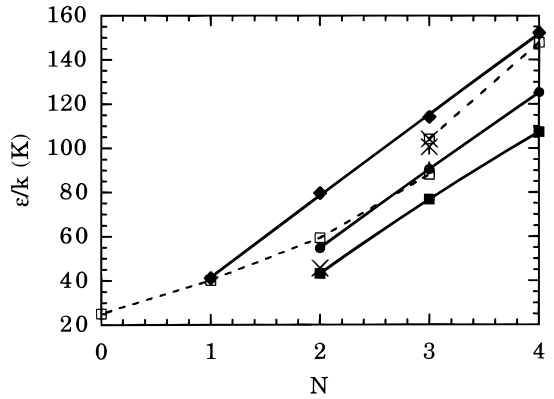

Figure 7. Well depth at 450 K vs number of hydrogens in the UA site. The open squares are from Jorgensen et al.[10] The X's are from Nath et al.[5] The filled squares are the LJ fits of the LJ-MOG averages. The filled circles are the LJ fits of the MOG averages. The filled diamonds are the LJ fits of the SLKB averages. Where available, CH_2 results for both ethane and *n*-butane are reported.

MOG and LJ-MOG explicit atom-derived potentials at 300 K. This is gratifying, not only because the united atom potentials were obtained from experimental PVT measurements assuming a Lennard-Jones form but also because experimental data are generally in the region near room temperature. Not surprisingly, our united atom potentials show some temperature dependence. This can be seen in Figure 7 at $T = 450$ K. The MOG derived united atom potentials are now more in agreement with recent parameters.[4,5] Incidentally, the apparent disagreement of the SLKB potential with standard UA potentials may be an artifact of our very approximate mapping to the Lennard-Jones 6−12 form. Indeed, the SLKB generated UA potential for methane gives excellent values for the second virial coefficient.

To put our numerical EA/UA mapping results in a usable form, we found that we could, to a good approximation, fit the data with a stretched exponential function of the form

$$u(r) = \epsilon\left[\left(\frac{6}{\eta\zeta - 6}\right)\exp\left[\zeta(1 - (r/R_0)^{\eta}) - \left(\frac{\eta\zeta}{\eta\zeta - 6}\right)(r/R_0)^{-6}\right]\right] \quad (4.2)$$

Table 6. Mapped United Atom Potentials for CH_4 (500 K > T > 200 K)

parameter	m_1	m_2	m_3
Mayo, Olafson, Goddard (LJ 6−12)			
R_0	4.402	3.519	0.053 96
ϵ	134.3	216.1	0.068 58
ζ(exp-6)	20.88	10.13	0.001 072
ζ	7.775	0.3184	0.014 96
η	2.773	11.40	0.122 8
Mayo, Olafson, Goddard (exp-6)			
R_0	4.308	3.737	0.043 16
ϵ	141.5	203.6	0.064 18
ζ(exp-6)	14.54	9.102	0.013 46
ζ	12.10	4.278	0.000 519 3
η	2.017	3.724	0.004 089
Sorensen, Liau, Kesner, Boyd (exp-6)			
R_0	4.162	3.588	0.057 18
ϵ	158.8	214.6	0.062 17
ζ(exp-6)	13.35	8.335	0.017 73
ζ	24.17	4.961	0.000 0495 1
η	1.740	3.0077	0.004 085

Table 7. Mapped United Atom Potentials for CH_3 (500 K > T > 200 K)

parameter	m_1	m_2	m_3
Mayo, Olafson, Goddard (LJ 6−12)			
R_0	4.424	3.907	0.057 74
ϵ	109.4	76.48	0.114 7
ζ(exp-6) = 14.21 + 0.005318T			
ζ	8.827	1.614	0.003 842
η	2.773	11.40	0.122 8
Mayo, Olafson, Goddard (exp-6)			
R_0	4.326	3.862	0.095 39
ϵ	115.1	86.5	0.050 59
ζ(exp-6) = 14.11 + 0.002415T			
ζ	9.645	2.312	0.001 902
η	2.455	6.896	0.008 038
Sorensen, Liau, Kesner, Boyd (exp-6)			
R_0	4.187	3.050	0.217 2
ϵ	131.6	105.3	0.026 51
ζ(exp-6) = 13.225 + 0.001676T			
ζ	10.00	2.598	0.001 598
η	2.135	5.963	0.007 742

involving the three exp-6 parameters plus an additional parameter η, which is a measure of steepness of the repulsive branch. This form is particularly useful at low temperature. Furthermore, we found that the temperature dependence of these four parameters usually could be expressed as

$$\text{parameter}(T) = m_1 - (m_1 - m_2)\exp[-(m_3 T)^{1/2}] \quad (4.3)$$

in the range 200 K < T < 500 K. The fitting parameters that summarize our numerical results are tabulated in Tables 6−9, although, for work of high accuracy, we recommend that the reversible work be explicitly computed. The units of these parameters are as follows: R_0 [Å], ϵ [K], ζ [unitless], η [unitless], and $u(r)$ [K].

The fitting process consisted of two phases. First, the minimum location and well depth were selected from the (numerical) reversible work function. Next, the steepness parameters, ζ and η, were chosen to best describe the function $\exp[-\beta w(r)]$. In this manner, large values of $w(r)$ were not unduly weighted in the fitting process. For temperatures over 200 K, the potential parameters vary by a relatively small amount. Because these variations are small, it is not surprising that a temperature-independent UA potential can be successful at modeling liquid−vapor equilibrium.

Table 8. Mapped United Atom Potentials for CH_2 (500 K > T > 200 K)

parameter	m_1	m_2	m_3
Mayo, Olafson, Goddard (LJ 6−12)			
R_0	4.447	3.357	0.117 4
ϵ	86.88	82.50	0.087 40
ζ(exp-6)	23.62	15.58	0.001 252
ζ	10.73	0.3024	0.006 160
η	2.542	10.18	0.023 39
Mayo, Olafson, Goddard (exp-6)			
R_0	4.365	1.532	0.262 8
ϵ	90.48	81.49	0.026 20
ζ(exp-6) = 16.78 + 0.002011T			
ζ	11.20	2.367	0.002 071
η	2.012	7.205	0.006 654
Sorensen, Liau, Kesner, Boyd (exp-6)			
R_0	4.222	2.235	0.278 3
ϵ	104.9	90.7	0.027 97
ζ(exp-6) = 15.56 + 0.000895T			
ζ	12.71	1.711	0.001 599
η	1.590	7.866	0.008 326

Table 9. Mapped United Atom Potentials for CH (500 K > T > 200 K)

parameter	m_1	m_2	m_3
Mayo, Olafson, Goddard (LJ 6−12)			
R_0 = 4.405			
ϵ	67.13	42.16	0.02405
ζ(exp-6)	25.16	6.785	0.01041
Mayo, Olafson, Goddard (exp-6)			
R_0	4.331	4.091	0.1176
ϵ	67.82	−794.6	0.6545
ζ(exp-6) = 17.816 + 0.003279T			
ζ = 4.798 + 0.003895T			
η = 6.692 − 0.005118T			
Sorensen, Liau, Kesner, Boyd (exp-6)			
R_0	4.183	4.379	0.02213
ϵ	79.58	39.36	0.07250
ζ(exp-6) = 16.466 + 0.003410T			
ζ = 3.829 + 0.007218T			
η = 7.193 − 0.008031T			

A natural result of our mapping procedure is that the UA potentials have a temperature dependence. Such behavior is not unknown in UA representations of molecules. Recently, Sun and Teja[11] have modeled alkanes as Lennard-Jones spheres with one sphere representing one molecule. As theirs is a much harsher treatment of the potentials, they find much larger temperature effects than we do in most cases. However, they also model methane where the rate of change of the well depth is in good agreement with the results of the present study.

In addition, our mapping implies that the effective hard core diameters of the united atom potentials have a complex temperature dependence. We computed this effective hard core diameter using the Barker−Henderson[12] expression

$$d = \int_0^\infty \{1 - \exp[-\beta w_0(r)]\}\, dr \quad (4.4)$$

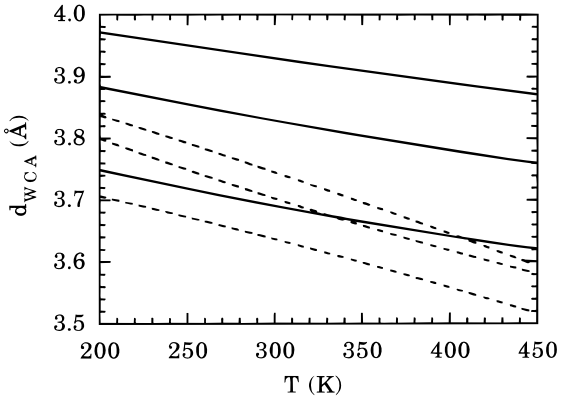

Figure 8. Variation of hard site diameter with temperature for the CH_2 UA potential. The solid lines are for the full averaged potentials. The dashed lines are for the Lennard-Jones fits to these averages. In order of decreasing site sizes these represent MOG-LJ, MOG, and SLKB.

where $w_0(r)$ is the reference part of the united atom potential using the Weeks−Chandler−Andersen[13] decomposition of the potential into a reference and perturbative part. The quantities $d(T)$ and $B(T)$ are tabulated for the various united atom potentials in Tables 2−5.

In Figure 8 we have plotted the hard core diameter as a function of temperature for a CH_2 site. The solid curves are from the full mapping procedure using the various explicit atom potentials. The dashed curves are from the Lennard-Jones united atom mapping discussed above. Clearly, the explicit atom derived potentials give a considerably higher hard core potential than does its "equivalent" Lennard-Jones form. In addition, it can be seen that the SLKB potential gives lower hard core diameters, not a surprising result since the R_0 values were also lowest with this potential.

In this work we employed three of the better known explicit atom potentials in our calculations. As improved explicit atom potentials become available, similar calculations can easily be performed to map onto united atom potentials. We hope that this will provide a useful and expedient guide in the development of both EA and UA potentials. It permits EA potentials, which are usually heavily influenced by low-temperature, crystal structures, to be benchmarked against UA potentials that have been developed specifically to model high-temperature phase behavior. On the other hand, it also supplies UA potentials with functional forms which more accurately reflect the UA site's composite behavior.

Acknowledgment. The part of this work performed at Sandia National Laboratories was supported by the U.S. Department of Energy under Contract DE-AC04-94AL85000.

References and Notes

(1) Allen, M. P.; Tildesly, D. J. *Computer Simulations of Liquids*; Oxford: New York, 1987.
(2) Schweizer, K. S.; Curro, J. G. *Adv. Chem. Phys.* **1997**, *98*, 1.
(3) Pant, P. V. K.; Han, J.; Smith, G. D.; Boyd, R. H. *J. Chem. Phys.* **1993**, *99*, 597.
(4) Siepmann, J. I.; Karaborni, S.; Smit, B. *Nature* **1993**, *365*, 330. Smit, B.; Karaborni, S.; Siepmann, J. I. *J. Chem. Phys.* **1995**, *102*, 2126. Siepmann, J. I.; Karaborni, S.; Smit, B. *J. Am. Chem. Soc.* **1993**, *115*, 6454. Martin, M. G.; Siepmann, J. I. *J. Am. Chem. Soc.* **1997**, *119*, 8921. Martin, M. G.; Siepmann, J. I. *J. Phys. Chem. B* **1998**, *102*, 2577.
(5) Nath S. K.; Escobedo, F. A.; de Pablo, J. J. *J. Chem. Phys.* **1998**, *108*, 9905.
(6) Mayo, S. L.; Olafson, B. D.; Goddard III, W. A. *J. Phys. Chem.* **1990**, *94*, 8897.
(7) Sorensen, R. A.; Liau, W. B.; Kesner, L.; Boyd, R. H. *Macromolecules* **1988**, *21*, 200. For corrections, see: Smith, G. D.; Yoon, D. Y. *J. Chem. Phys.* **1994**, *100*, 649.
(8) McCoy, J. D.; Mateas, S.; Zorlu, M.; Curro, J. G. *J. Chem. Phys.* **1995**, *102*, 8635.
(9) See, for instance: Chandler, D. *Introduction to Modern Statistical Mechanics*; Oxford: New York, 1987.
(10) Jorgensen, W. L.; Madura, J. D.; Swenson, C. J. *J. Am. Chem. Soc.* **1984**, *106*, 6638.
(11) Sun, T.; Teja, A. S. *J. Phys. Chem.* **1996**, *100*, 17365. Sun, T.; Teja, A. S. *Ind. Eng. Chem. Res.* **1998**, *37*, 3151.
(12) Barker, J. A.; Henderson, D. *J. Chem. Phys.* **1967**, *47*, 4714. Barker, J. A.; Henderson, D. *Annu. Rev. Phys. Chem.* **1972**, *23*, 439. Barker, J. A.; Henderson, D. *Rev. Mod. Phys.* **1976**, *48*, 587.
(13) Andersen, H. C.; Weeks, J. D.; Chandler, D. *Phys. Rev. A* **1971**, *4*, 1597. Weeks, J. D.; Andersen, H. C.; Chandler, D. *J. Chem. Phys.* **1971**, *54*, 5237. Weeks, J. D.; Andersen, H. C.; Chandler, D. *Adv. Chem. Phys.* **1976**, *34*, 105.
(14) Hirschfelder, J. O.; Curtiss, C. F.; Bird, R. B. *Molecular Theory of Gases and Liquids;* Wiley and Sons: New York, 1954.
(15) Ben-Amotz, D.; Herschbach, D. R. *J. Phys. Chem.* **1990**, *94*, 1038.
(16) van der Vegt, N. F. A.; Briels, W. J.; Wesslig, M.; Strathmann, H. *J. Chem. Phys.* **1993**, *105*, 8849.
(17) Matyushov, D. V.; Schmid, R. *J. Chem. Phys.* **1996**, *104*, 8627.
(18) Dunfield, L. G.; Burgess, A. W.; Scheraga, H. A. *J. Phys. Chem.* **1978**, *82*, 2609.
(19) Jorgensen, W. L. *J. Am. Chem. Soc.* **1981**, *103*, 335, 341, 345.
(20) Lopez-Rodriguez, A.; Vega, C.; Freire, J. J.; Lago, S. *Mol. Phys.* **1991**, *73*, 691. Lopez-Rodriguez, A.; Vega, C.; Freire, J. J.; Lago, S. *Mol. Phys.* **1993**, *80*, 1565.
(21) Ryckaert, J.-P.; Bellmans, A. *Faraday Discuss. Chem. Soc.* **1978**, *66*, 95.
(22) Weber, T. A.; Helfand, E. *J. Chem. Phys.* **1979**, *71*, 4760.
(23) Daura, X.; Mark, A. E.; van Gunsteven, W. F. *J. Comput. Chem.* **1998**, *19*, 535.

MA981060G